Degradation of zinc oxide thin films in aqueous environment: Part I – Bare Films

Degradation von dünnen Zinkoxidfilmen in wässriger Umgebung: Teil I – Ungeschützte Filme

L. De Rosa, N. Perugini, D. B. Mitton, T. Monetta, F. Bellucci* and J. Springer

As their optical, electrical, and electrochemical properties can be modified, zinc oxide thin films are employed as optically transparent conductors in the production of many different microdevices. Although microdevices are generally encapsulated for protection from aggressive environment, the zinc oxide thin films can still degrade with a resultant decrease in device performance. The investigation of the mechanism of degradation for these films is, therefore, of significant interest in prolonging the lifetime of many electronic devices.

In this paper, the behaviour of bare zinc oxide thin films produced by magnetron-sputtering (MS-ZnO) and exposed to aqueous aerated 3.5% NaCl at 25 °C was investigated. Scanning Electron Microscopy (SEM), Electrochemical Impedance Spectroscopy (EIS) and DC measurements were employed to study the degradation mechanisms of two sputtered-ZnO films having different microstructures. The experimental tests were primarily focused on defining the relationship between microstructure and the degradation rate of the ZnO thin films.

Due to the development of moisture induced microfractures in the ZnO films, a two stage mechanism was suggested. Two different equivalent electrical circuits are, thus, proposed to interpret the EIS data at different stages in the degradation. The parameters of the equivalent network were related to degradation development, the change of degradation mechanism and the extent of microfracture in the film.

Zinkoxidschichten werden wegen ihrer besonderen optischen, elektrischen und elektrochemischen Eigenschaften für wichtige Funktionen verschiedener elektronischer Komponenten als transparente leitfähige Schichten eingesetzt. Obwohl solche Komponenten im allgemeinen zum Schutz gegen Umwelteinflüsse verkapselt sind, hat es sich gezeigt, dass diese Schichten degradieren können und damit die Funktion des Geräts beeinträchtigt werden kann. Die Untersuchung der Degradationsmechanismen ist daher von großem Interesse für die Verlängerung der Lebensdauer dieser Geräte.

In der vorliegenden Arbeit wurde das Verhalten von ungeschützen Zinkoxidschichten, die mit dem Magnetronsputterprozess hergestellt wurden, unter dem Einfluss von luftgesättigter, 3,5%iger wässriger Kochsalzlösung untersucht. Rasterelektronenmikroskopie (REM), Elektrochemische Impedanzspektroskopie und DC-Messungen wurden angewandt, um den Degradationsmechanismus von zwei gesputterten ZnO-Schichten aufzuklären. Die Untersuchungen waren vor allem auf den Zusammenhang zwischen Mikrostruktur und Alterungsgeschwindigkeit der ZnO-Schichten konzentriert.

1 Introduction

Thin films of ZnO obtained by magnetron sputtering (MS) are largely employed for the production of transparent and electrically conductive devices [1–6].

1.1 Morphology of MS ZnO

ZnO thin films produced by magnetron sputtering, ranging from 0.2 to 1 μm in thickness reveal nanocrystalline morphology. Crystals tend to be columnar and hexagonal with diameters ranges from 50 to 400 nm, and with the longitudinal axis oriented perpendicular to the substrate (preferential orientation is along the 0001 axis) [2, 3]. This morphology has been observed for different deposition conditions and for both amorphous and crystalline substrates [2, 3].

1.2 Electrical properties of MS ZnO

Zinc oxide crystals are non-stoichiometric compounds having an excess of zinc content, ZnO_{1-x}. According to the literature, the electrical conduction of pure ZnO is primarily due to the non-stoichiometric excess of Zn^+ interstitially dissolved in the crystal lattice and to a smaller extent to oxygen vacancies [1–3]. Both these lattice defects lead to n-type conductive oxide; however, experimental evidence of higher contribution of interstitial Zn ions is reported in the scientific literature [1].

In the case of microcrystalline ZnO, the electrical behavior of the thin film is mainly dependant on the morphology and can significantly differ from that of single crystals [2, 5]. The

* *F. Bellucci, L. De Rosa, N. Perugini, D. B. Mitton, T. Monetta*
Dep. of Materials and Production Engineering – University of Naples Federico II
P.le Tecchio 80, I-80125 Napoli (Italy)

J. Springer
Zentrum fur Sonnenenergie und Wasserstoff-Forschung, Baden-Württemberg
Hessbrühlstrasse 21C, D-70565 Stuttgart (Germany)

0947-5117/01/1111-0844$17.50+.50/0

number and mobility of charge carriers decrease with micrograins size and strongly depends on the micrograins orientation. There is evidence reported in the literature of an oxygen excess at the ZnO grain boundaries [2, 5]. This effect can produce p-type semiconducting in nanocrystalline ZnO, due to the huge grain boundary area of the film [2].

The number of charge carriers is also related to the ratio between the oxygen and zinc concentration in the oxide. Therefore, in the magnetron sputtering process the oxygen partial pressure in the deposition chamber can be employed to tailor the conductivity of the film.

1.3 Electrochemical properties

The Zinc oxide/electrolyte interface has been extensively investigated in the case of single crystals [6, 7]. According to classical theory of a semiconducting electrode and to the experimental results reported in literature, space distributed charge excess exists both in the electrolyte and in the semiconductor. In the semiconducting phase, the excess charge is both (i) localized surface states and (ii) distributed in a region extending from the interface to the bulk of the semiconductor, the space charge region [8]. The charge surface states, however, can be neglected at a single crystal ZnO/electrolyte interface [6, 7, 9]. Charge transfer and electrochemical reactions at the electrolyte/semiconductor interface was shown to be negligible (blocking electrode behavior) for ZnO single crystals [6, 7].

Results, obtained on bulk single crystal ZnO, can be applied only in a limited way to MS-ZnO films. Due to their nanocrystalline structure, the latter have a significant grain boundary area, which can profoundly influence the electrochemical behavior [2]. There are numerous reports of these differences in the literature. The structure of MS-ZnO/electrolyte was shown to be non-blocking at both acid and basic pH values due to the higher reactivity of the polycrystalline morphology of the oxide [2, 6, 7]. The thickness of the thin films (10 – 100 nm) is comparable to the expected extension of the space charge region ($10 - 10^3$ nm [3, 8]) showing, thus, a space charge capacitance higher than the expected values for a semi-infinite medium. Finally, the contribution of surface states to the total capacitance is higher for polycrystalline ZnO than for single crystals [2, 6, 7].

1.4 Degradation

While the electrical and electrochemical properties of the "as produced" zinc oxide thin films have been extensively reported in the literature, their stability during the operating life of a device remains an open matter. It has previously been reported that zinc oxide thin films are subject to changes in their electrical properties when exposed to high humidity or to an electrolytic solution [10]. These phenomena are related to the diffusion of charge carriers from the oxide to the environment, and to the electrochemical reactions occurring at the moisture/ZnO interface. A recent investigation indicated that the electrode behavior of a polycrystalline zinc oxide is strictly related to the pH of the solution [2]. In the high pH range, the oxide reacts with hydroxyl ions producing zinc hydroxide by the following hole transfer reaction: $ZnO + OH^- + 2\,h^+ \rightarrow Zn(OH)^+ + 1/2\,O_2$, while in the low pH range the zinc oxide dissolves to give divalent ions, as in the following reaction: $ZnO + 2\,h^+ \rightarrow Zn^{++} + ½\,O_2$. No experimental results were found in the literature regarding the degradation of ZnO for neutral pH conditions. Recent investigations by photoelectrochemical and photoinduced microwave techniques indicate that MS-ZnO electrodes are more reactive than single crystal ZnO electrodes. Reportedly, this is due to their polycrystalline morphology and to the high number of reactive surface sites [11 – 16]. This behavior exhibits a strong dependance on crystal morphology and deposition technique.

In the subsequent sections, some experimental evidence of the degradation mechanism of MS-ZnO thin films during exposure to aqueous 3.5% NaCl will be presented.

2 Materials and methods

Magnetron sputtered zinc oxide thin films were produced by Zentrum für Sonnenenergie und Wasserstoff-Forschung, Stuttgart by using a semicontinous reactor. The deposition was carried out on a $10 \times 10\,cm^2$ sodium glass panel and a mask was employed to obtain a striped configuration of the thin film. On each glass panel, four stripes ($1 \times 10\,cm^2$) were obtained. The ZnO growth was carried out until a 0.5 micron layer was obtained. In this paper, ZnO thin film, obtained using two different proprietary sets of parameters (temperature and oxygen partial pressure), were investigated. In subsequent sections of this paper, the different sets of deposition parameters have been termed Condition a and Condition b and the related thin film produced by employing these conditions are designated as a-ZnO and b-ZnO.

The degradation of ZnO samples exposed to an aqueous 3.5% NaCl solution at 25 °C was investigated by (i) Scanning Electron Microscopy (SEM), (ii) Electrochemical Impedance Spectroscopy (EIS) and (iii) DC current measurement.

EIS measurements were performed by employing a Solartron 1260 Frequency Response Analyser (FRA) in combination with a Solartron 1286 potentiostat. Measurements were made in the frequency range $0.02 - 10^5$ Hz, during exposure to an aqueous aerated 3.5% NaCl solution at 25 °C. A dark chamber was employed to avoid any photoconductive effect at the ZnO electrode during the EIS experiment [14].

The DC resistivity of both a-ZnO and b-ZnO was monitored by a PC-driven Keithley multimeter during exposure in a humidity chamber (Weiss-Gerätetechnik Kälte-Wärme Prüfschrank Mod. 305SB) at 85% R.H. and 85 °C. Further information on the experimental apparatus has previously been reported in literature [10].

3 Results and discussion

3.1 Morphology

As reported in the introduction, MS-ZnO thin films exhibit columnar nanocrystalline morphology. The temperature of the substrate and the atmosphere composition in the deposition chamber, however, have an influence on the growth and final morphology of the ZnO nanocrystals.

The surface and the cross-section of the "as produced" a-ZnO thin film are reported in Fig. 1(a) and 1 (b), respectively. As seen in Fig. 1(a), the surface of the a-ZnO reveals significant nano-roughness and preferential orientation. The nano-roughness is representative of the upper surface of the columnar grains; however, it was not possible to resolve the hexagonal crystal structure during SEM analysis. The a-ZnO cross

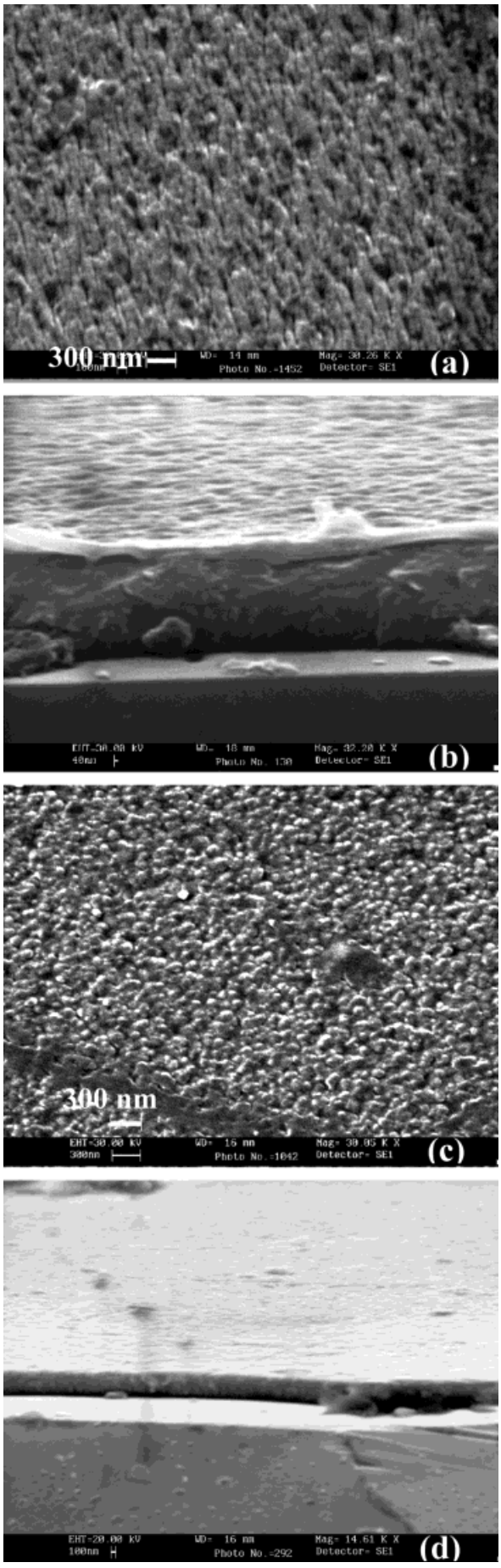

section, reported in Fig. 1(b), indicates a structure composed of two layers, with both a 500 nm lower layer and a 50 nm upper layer clearly discernible. The surface of b-ZnO, as presented in Fig. 1(c), also reveals significant nano-roughness; however, in this case, the upper surface of columnar crystals is more clearly recognizable and a mean diameter in the range of 50 – 100 nm was determined. While both films are visually transparent, the a-ZnO films display a yellowish tint but the b-ZnO films are completely colorless.

3.2 Degradation

Both, a-ZnO and b-ZnO samples experience degradation and structural changes when exposed to aqueous 3.5% NaCl at ambient temperature.

The surface of the a-ZnO thin film at different stages of exposure to the test solution is illustrated in Fig. 2(a – d). After 5 days of exposure, Fig. 2(a), in some discrete regions the upper layer appears to be well preserved (right side in the figure), while in other areas corrosion is apparent. In the corroded areas, the upper layer of the a-ZnO film appears to have degraded and the lower layer exhibits significant evidence of pitting (left side in the figure). In the regions where the upper layer is dissolved, the preferential orientation of the lower layer can be easily noticed. The same sample after 14 days of exposure shows advanced pitting, as illustrated in Fig. 2(b). The mean diameter of pits was in the order of 1 μm. At this stage the surface microstructure is smoother than that observed for the "as produced" sample, possibly as a result of generalized dissolution over major portions of the surface. After 37 days of exposure, Fig. 2(c), degradation is widespread with no distinct preserved regions apparent. At this stage, with much of the surface involved, pits are not easily identifiable. After 66 days of exposure, the morphology of the a-ZnO layer has changed (Fig. 2(d)) and exposed substrate is visible at the base of some pits, indicating that the entire layer thickness has been depleted.

The surface of b-ZnO thin film at different stages of exposure to aqueous 3.5% NaCl is illustrated in Fig. 3. As presented in Fig. 3(a), after 5 days of exposure, a fracture developed in the b-ZnO layer, with accompanying upward deformation of the thin film.

While any significant attempt to identify the correct fracture mechanism is beyond the scope of this work, it is likely attributable either to (i) a volume increase of b-ZnO (possibly as a result of the production of ZnOH from ZnO) and attendant compressive stress development within the thin film or to (ii) osmotic water pressure under the thin film and creation of upward forces. When the region around the fracture was observed at higher magnification (Fig. 3(b)), no evidence of corrosion was found and the surface texture appeared undegraded.

Fig. 1. SEM micrograph of "as grown" ZnO thin films: (a) surface of a-ZnO, (b) cross section of a-ZnO, (c) surface of b-ZnO, and (d) cross section of b-ZnO

Abb. 1. REM-Aufnahme einer frischen ZnO-Schicht: a) Oberfläche der Schicht „a-ZnO", (b) Querschnitt der Schicht „a-ZnO", c) Oberfläche der Schicht „b-ZnO", (d) Querschnitt der Schicht „b-ZnO"

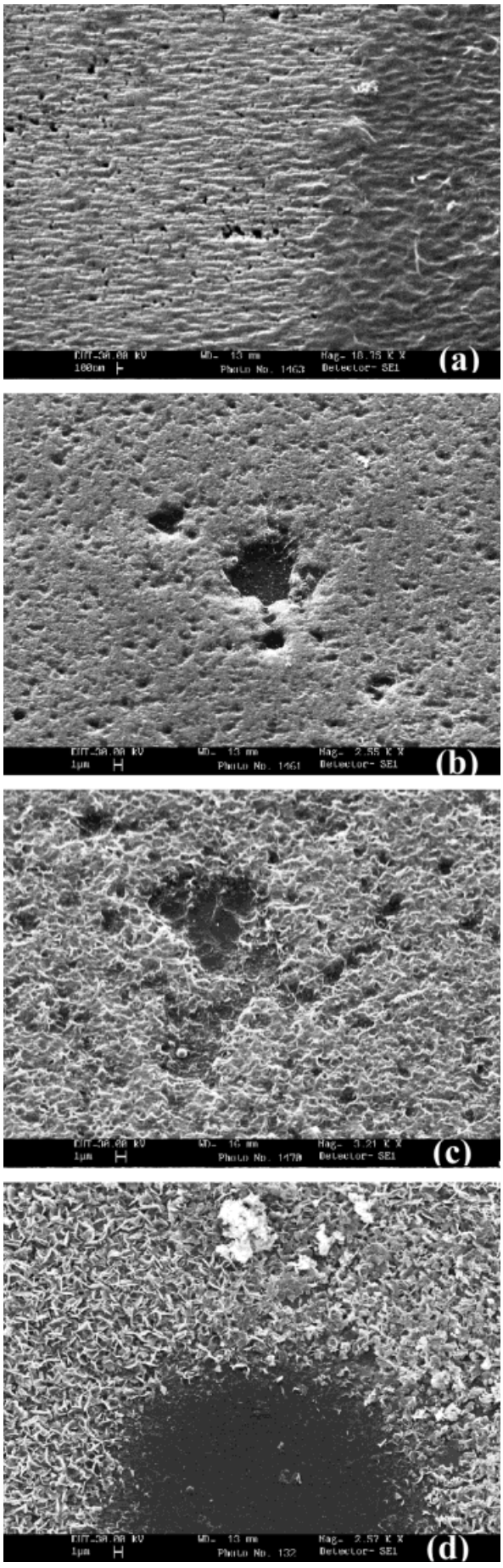

After 10 days of exposure (Fig. 3(c)), numerous fractures were distributed uniformly over the sample surface. The mean fracture length was in the range of 50 – 500 μm. At higher magnification, Fig. 3(d), fractures exhibiting upward borders and delamination of the thin film along the fracture line can clearly be recognized. This evidence suggests that the fracture phenomenon is driven by an upward stress and/or a compression stress parallel to the substrate layer. At this stage of exposure, however, the thin film microstructure is well preserved, and no indication of degradation of the nanocrystalline texture can be observed.

3.3 Impedance Spectra

Both a-ZnO and b-ZnO samples were assessed by EIS at the open circuit potential (ocp) as a function of exposure time in the test solution. The Bode magnitude and phase angle spectra for a-ZnO thin films are presented as a function of time in Fig. 4(a) and Fig. 4(b), respectively. For short exposure times ($t = 1$ h), the impedance spectrum indicate a single time constant, with pseudocapacitance behavior in the lower frequency region and resistive behavior in the high frequency region. The absence of resistive behavior in the low frequency region suggests that the a-ZnO thin film is behaving as a blocking electrode. The influence of diffusion and/or relaxation phenomena can be recognized in the phase diagram at the lowest frequencies (0.02 – 5 Hz), where the phase angle decreases with decreasing frequency. After 9 days of exposure, the impedance still exhibits a single time constant and a shape similar to the 1 h spectrum. On the other hand, the pseudocapacitance value has increased by approximately a half order of magnitude. As can be observed by the phase diagram, the influence of relaxation or diffusion phenomena is less evident at this stage, and it confined to the lowest frequency region (0.02 – 0.1 Hz). Non-ideal behavior of the capacitance is, however, still evident since the phase angle maximum is around 83°. After 31 days of exposure, one time constant is still evident and the pseudocapacitance exhibits a further increase. In the phase angle diagram, the relaxation/diffusion phenomena are no longer easily distinguishable. After 52 days of exposure, a second time constant can easily be observed in the mid frequency range (1 – 1000 Hz) both in the magnitude and in the phase angle diagram. At this stage of exposure: (i) the relaxation/diffusion related phenomena have completely disappeared, (ii) further changes in the low frequency pseudocapacitance are not observed, and (iii) a significant increase in the value of the high frequency plateau can be observed. After 64 days of exposure the second time constant can easily be identified both in the impedance spectra and in the phase angle diagram.

The Bode magnitude and phase angle spectra for b-ZnO thin films are presented as a function of time in Fig. 4(c) and Fig. 4(d), respectively. Short duration data (1 h) again reveal a single time constant, and comments made previously

Fig. 2. SEM micrograph of a-ZnO thin films at different stages of exposure to 3.5%w NaCl acqueous solution: (a) after 5 days of exposure; (b) after 10 days of exposure; (c) after 37 days of exposure; and (d) after 66 days of exposure

Abb. 2. REM-Aufnahme der Schicht „a-ZnO“ nach verschiedenen Stadien der Behandlung mit 3,5%iger wässriger NaCl-Lösung: (a) nach 5 Tagen; (b) nach 10 Tagen; (c) nach 37 Tagen; (d) nach 66 Tagen der Behandlung

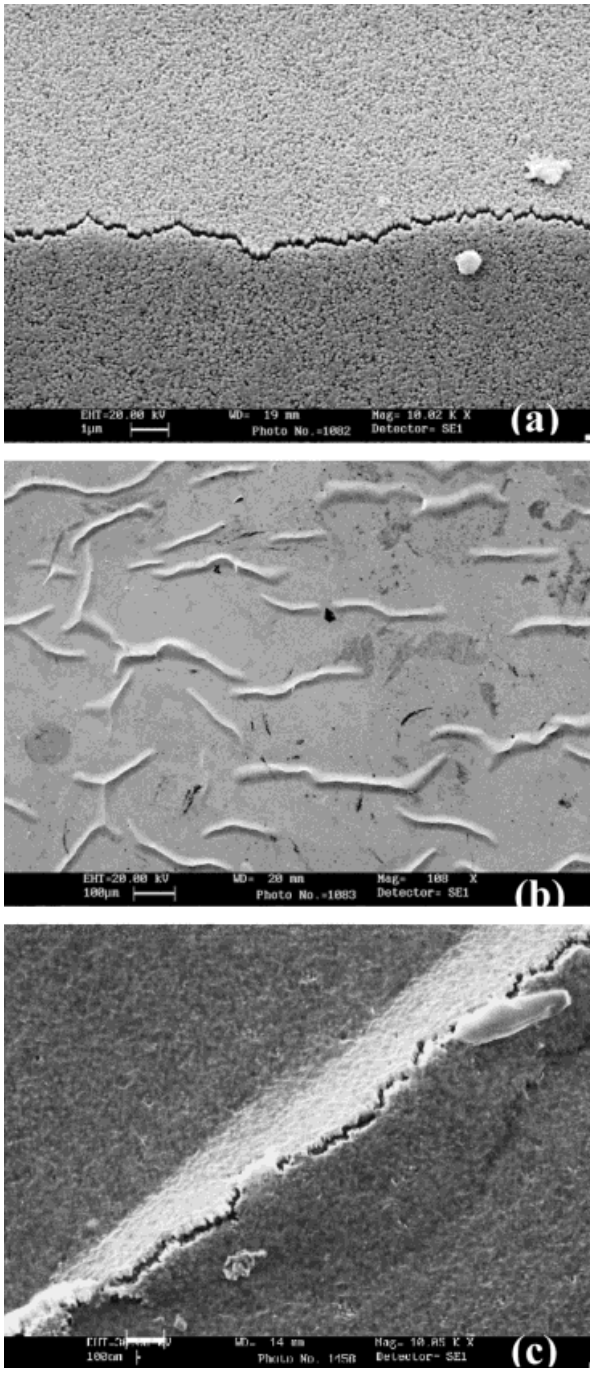

Fig. 3. SEM micrograph of b-ZnO thin films at different stages of exposure to 3.5%w NaCl acqueous solution: (a) after 5 days of exposure; (b,c) after 10 days of exposure

Abb. 3. REM-Aufnahme der Schicht „b-ZnO" nach verschiedenen Stadien der Behandlung mit 3,5%iger wässriger NaCl-Lösung: (a) nach 5 Tagen; (b, c) nach 10 Tagen der Behandlung

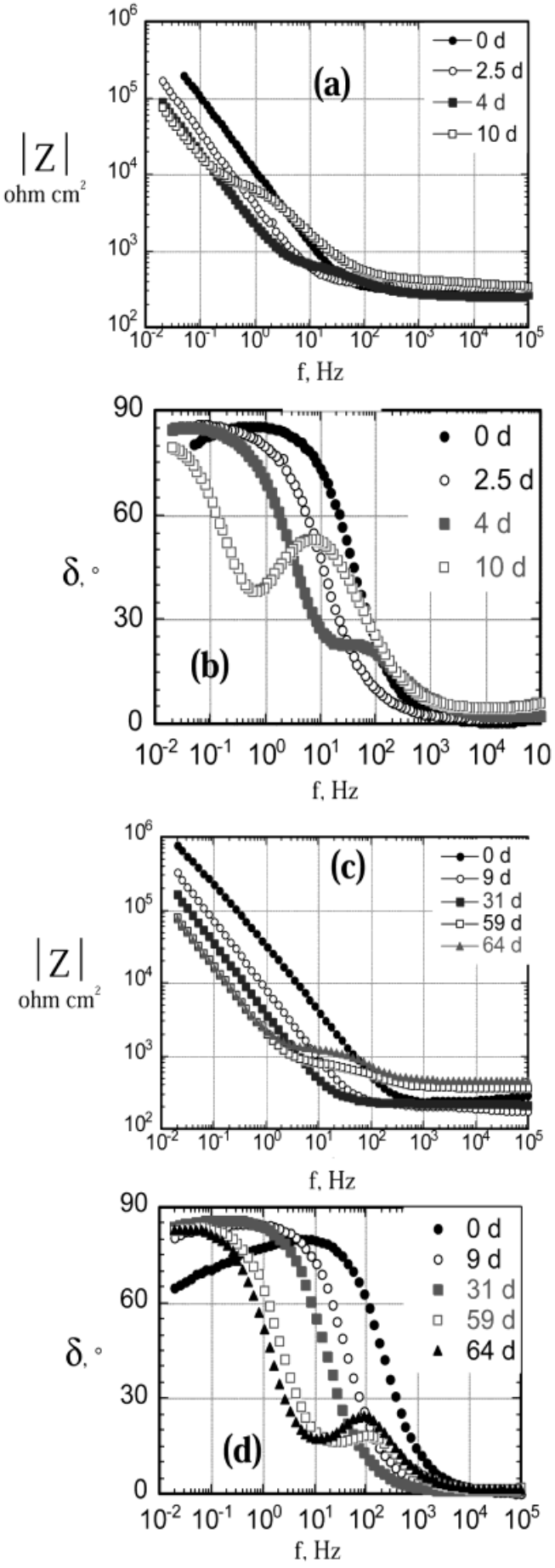

Fig. 4. Impedance spectra and phase diagram for a-ZnO thin film (inserts a and b) and b-ZnO thin film (inserts c and d) reported at different times of exposure to 3.5%w NaCl aqueous solution at 25 °C

Abb. 4. Impedanzspektren und Phasendiagramm für die a-ZnO-Schicht (Teilbilder a und b) und die b-ZnO-Schicht (Teilbilder c und d) aufgezeichnet nach verschiedenen Behandlungszeiten mit 3,5%iger wässriger NaCl-Lösung bei 25 °C

for a-ZnO at an equivalent exposure time regarding pseudo-capacitance, resistive plateau, diffusion related phenomena and blocking behavior, are also valid in this case. After 3 days of exposure the data continues to indicate only one time constant and diffusion related phenomena are not apparent, even in the phase angle diagram. However, after 4 days of exposure, the rise of a second time constant was noted at medium frequencies, both in the magnitude and phase angle data. The second time constant developed with time and was even more pronounced after 10 days of exposure.

During this work, an apparent correlation was noted between the appearance of a second time constant and either (i) the penetration of pits to the substrate in the case of a-ZnO films, or (ii) the time required for advanced fracture in the case of b-ZnO. As illustrated in the subsequent section, the emergence of a second time constant in the impedance data is indicative of the development of discontinuities (pits or fractures) in the semiconductor layer.

3.4 Equivalent Circuits

From the impedance point of view, the electrochemical cell and the ZnO layer can be represented schematically by the electrical network reported in Fig. 5(a). The current flows from the counter electrode, through the solution and the ZnO layer to the external contact. The interfacial region can be viewed as being composed of infinitely small adjacent impedances $d\underline{Z}$ connected in series. A single dZ is assumed to be composed of (i) the double layer capacitance, dC_{SC}, (ii) the warburg impedance, dW, and (iii) the ZnO resistance, dR_{ZnO}, connected as indicated in the insert, Fig. 5(b). Charge transfer resistance was not taken into account in the circuit, due to the blocking behavior of ZnO electrode. This complex equivalent network can be simplified to the electrical circuit reported in Fig. 5(c). In this latter circuit R_{ZnO} is the electrical resistance of the ZnO layer, Q_{SC} is representative of the double layer polarization and W accounts for the diffusion related phenomena observed at low frequencies in the early stages of exposure.

During the latter stage of exposure, voids (either fractures or deep pits) constitute a significant portion of the thin film; thus, the electrical network reported in Fig. 6(a) may be employed to describe the electrochemical impedance. In this network, the warburg elements are neglected and the ZnO resistance, dR_{ZnO}, is replaced by a more complex impedance, $d\underline{Z}_{ZnO}$. This latter impedance takes into account that the ZnO layer contains voids filled by the electrolyte. Each void in the thin film is represented by a series RC circuit, as reported in Fig. 6(b). At higher frequency, the current flows through the voids, since the void capacitance exhibits low impedance at this frequency. At medium frequencies, however,

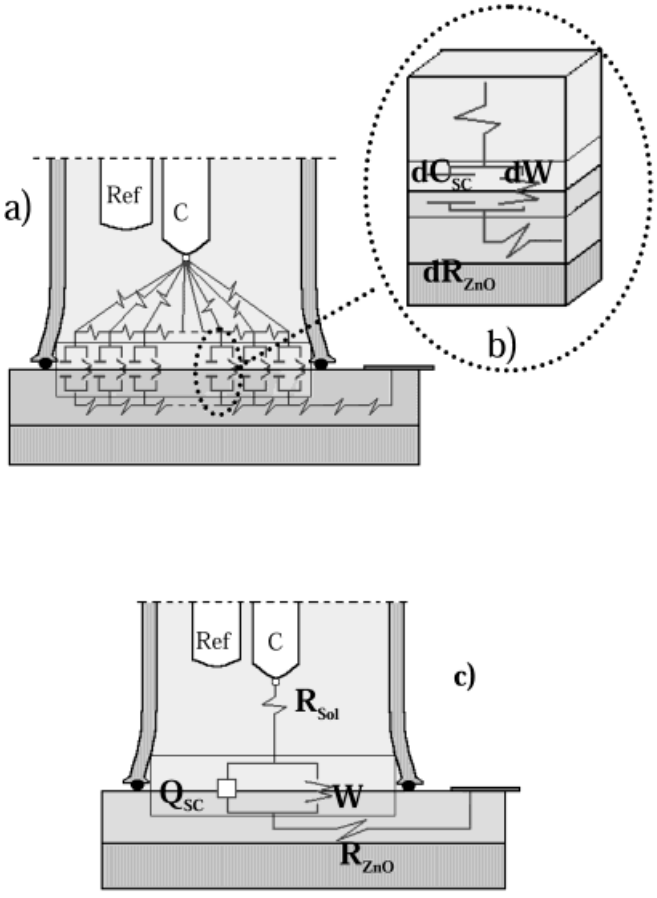

Fig. 5. EIS model employed for ZnO thin film before the fracture initiation: a) complete equivalent network and c) simplified equivalent circuit

Abb. 5. EIS-Modell für den ZnO-Film vor Beginn des Bruchs: a) vollständiges Ersatzschaltbild und c) vereinfachtes Ersatzschaltbild

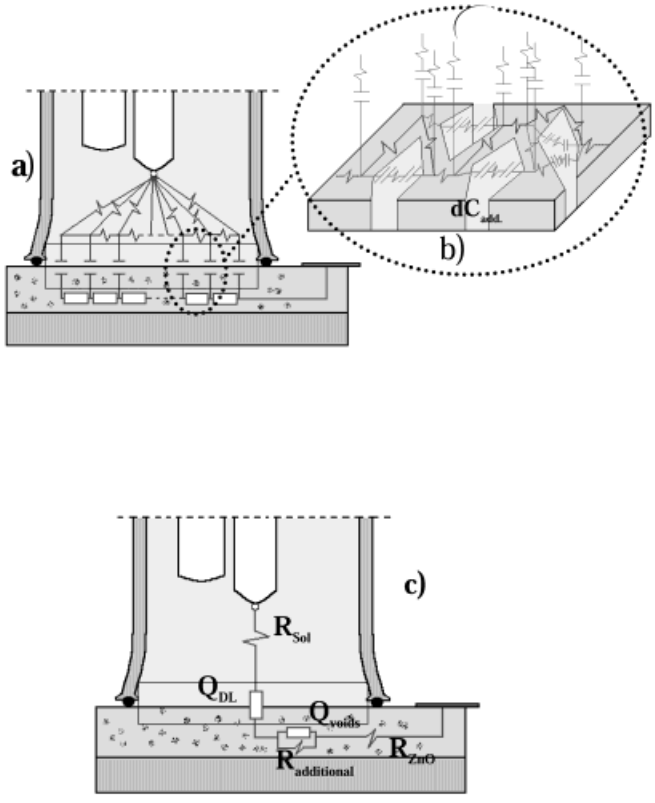

Fig. 6. EIS model employed for ZnO thin film after advanced pitting or fracture has taken place: a) complete equivalent network and c) simplified equivalent circuit

Abb. 6. EIS-Modell für den ZnO-Film nach fortgeschrittenem punktuellem Angriff oder Bruch: a) vollständiges Ersatzschaltbild und c) vereinfachtes Ersatzschaltbild

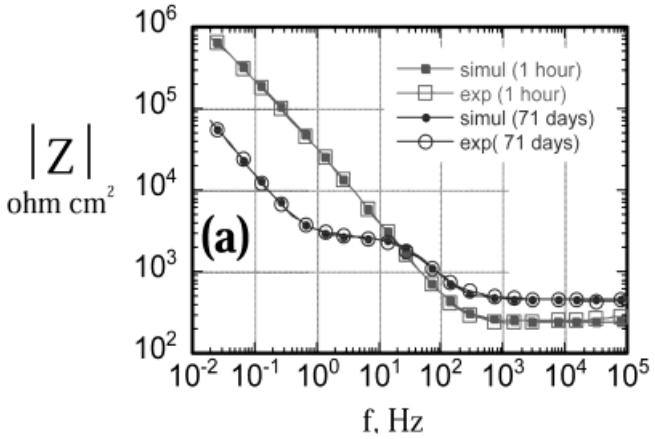

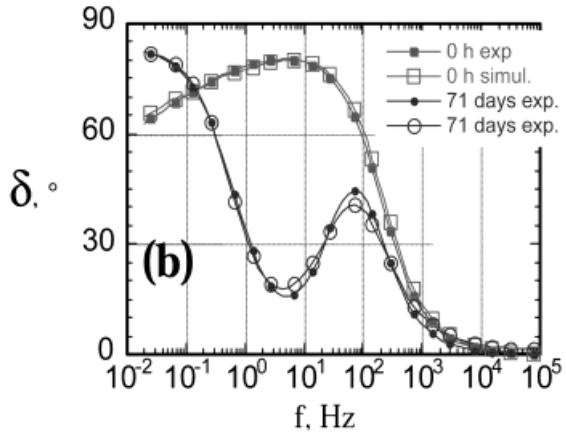

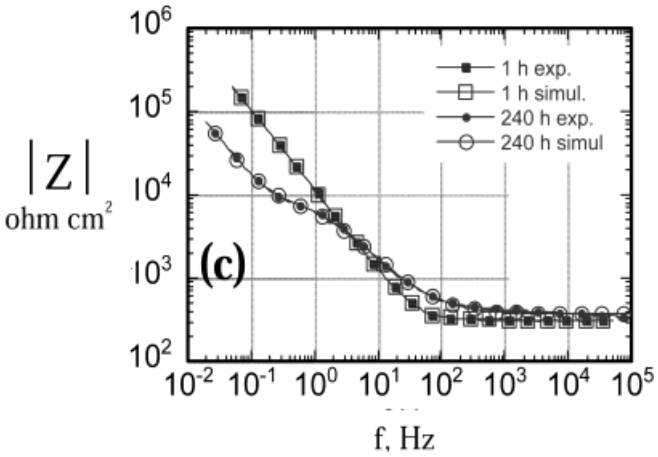

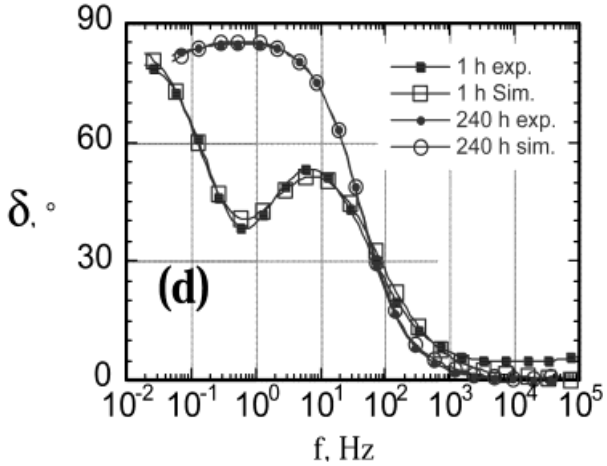

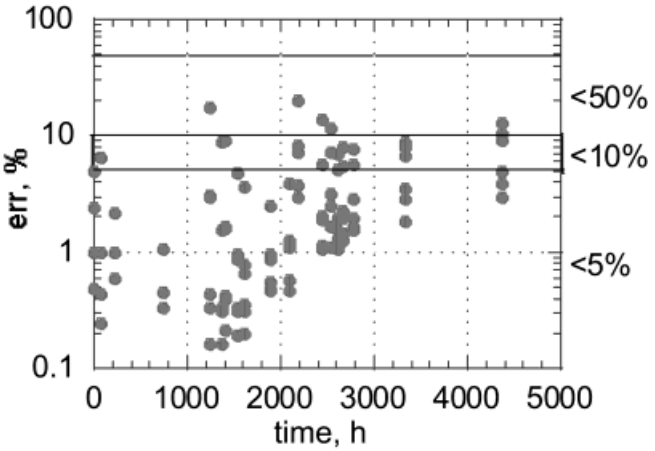

Fig. 8. Values of the fitting errors for all the data of a-ZnO (both at early and late stages of exposure)

Abb. 8. Werte der Abweichung der Anpassung für alle Messwerte von a-ZnO (sowohl im frühen als auch im späten Stadium der Behandlung)

since the void capacitance exhibits high impedance, the current flows around the voids (in the ZnO thin film). This latter shift of current flow explains the appearance of the second time constant in the impedance spectrum, reported in Fig. 4.

This complex electrical network can be simplified to the equivalent circuit reported in Fig. 6(c) where (i) R_{ZnO}, is the resistance of the ZnO in the regions between the voids, (ii) $R_{Additional}$ is the resistance of the ZnO around the voids, (iii) Q_{voids} accounts for the double layer phenomena in the voids and (iv) Q_{dl} accounts for the polarization phenomena on the whole surface.

The comparison between the simulated and experimental data at different stages of exposure is reported in Fig. 7 for both a-ZnO and b-ZnO. The experimental data show a good agreement with model predictions at any time of exposure, as can be noticed in Fig. 8 where parameter values and fitting errors are reported at different stage of exposures.

The trends for each dipole of the equivalent circuit as a function of the time of exposure are reported in Fig. 9 and Fig. 10. The resistance R_{ZnO}, reported in Fig. 9(a), shows a plateau during the early stages of exposure followed by a steep increase at later exposure times. In the case of b-ZnO the raise of R_{ZnO}, cannot be observed due to lack of data at longer times. The steep raise in R_{ZnO} observed for a-ZnO coincides with the appearance of the second time constant. At this stage the resistance $R_{Additional}$ can be measured, as presented in Fig. 9(b). This latter also increases with exposure time for both a-ZnO and b-ZnO. The pseudocapacitance, Q_{dl}, and its exponent, n_{dl}, are reported in Fig. 10(a) as $Q_{ZnO/Sol}$ and $n_{ZnO/Sol}$. During the early stages of exposure Q_{dl} increases with time, while n_{dl} is constant and close to 0.95 for both a-ZnO and b-ZnO. In the

Fig. 7. Comparison between experimental and theoretical impedance and phase diagram for (a, b) sample deposited under conditions A and (c, d) samples deposited under conditions B

Abb. 7. Vergleich zwischen experimentellem und theoretischem Impedanz- und Phasenverlauf für (a, b) Proben des Typs a-ZnO und (c,d) Proben des Typs b-ZnO

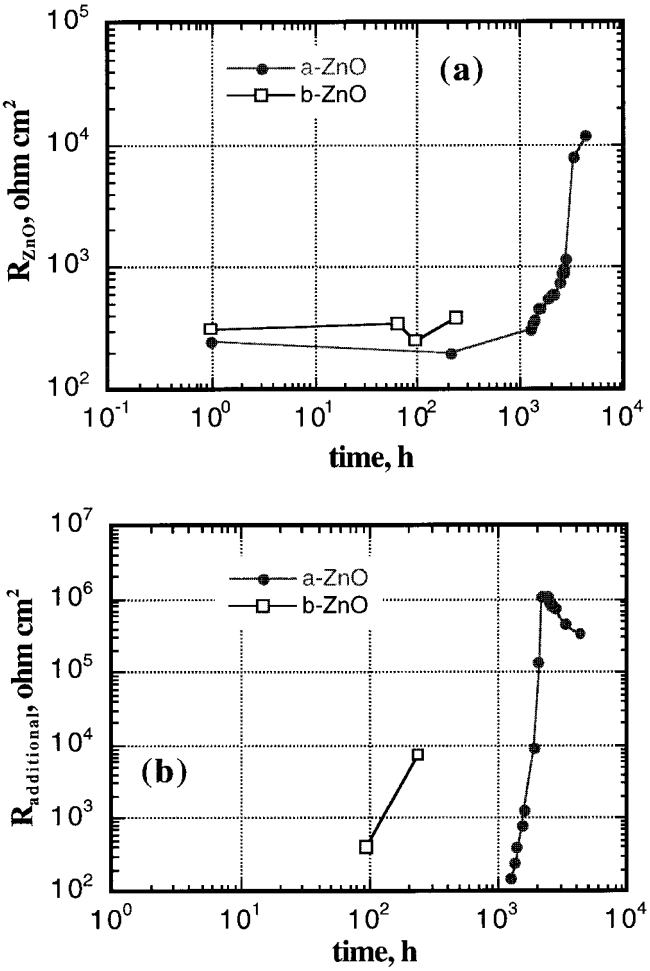

Fig. 9. Values of the circuital components reported as a function of exposure time: (a) R_{ZnO}; and (b) $R_{Additional}$

Abb. 9. Werte der Parameter des Ersatzschaltkreises als Funktion der Behandlungszeit: (a) R_{ZnO}; and (b) $R_{Additional}$

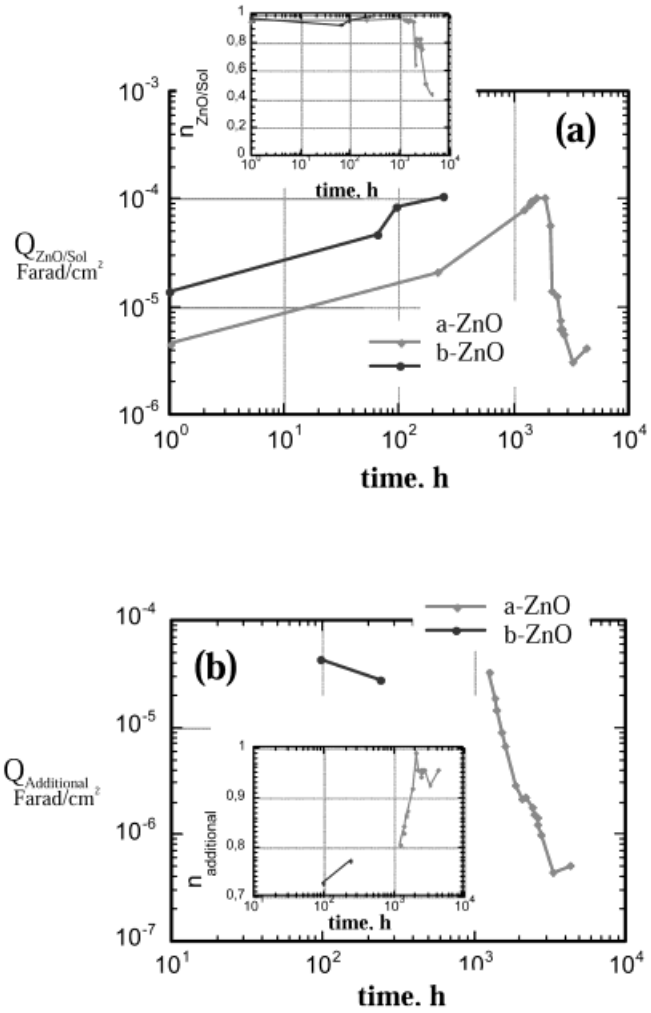

Fig. 10. Values of the circuital components reported as a function of exposure time: (a) Q_{dl} and n_{dl} and (b) Q_{voids} and n_{voids}

Abb. 10. Werte der Parameter des Ersatzschaltkreises als Funktion der Behandlungszeit: (a) Q_{dl} and n_{dl} and (b) Q_{voids} and n_{voids}

case of a-ZnO, however, a steep fall in Q_{dl} values concurrent with a similar fall in n_{dl} values is observed at later exposure times. Q_{voids}, and n_{voids} are reported in Fig. 10(b) as $Q_{Additional}$ and $n_{Additional}$. A steep fall in Q_{voids} concurrent with a raise in n_{voids} can be observed for both a-ZnO and b-ZnO. For a-ZnO, however, a deviation from this trend can be observed in n_{voids}.

As previously mentioned, R_{ZnO} is representative of the resistance of the ZnO film in the regions between the voids, while $R_{additional}$ is representative of ZnO resistance in the paths around the voids. Therefore, the sum of R_{ZnO} and $R_{additional}$ is representative of the total resistance of the ZnO sample measured by EIS (R_{EIS}). A comparison of R_{EIS} with the resistance measured by DC ohmmeter, R_{tester}, is reported in Fig. 11 for a-ZnO. It can be observed that at early stages there is a discrepancy between of about 50 ohms. At later stages, a good agreement can be observed between R_{EIS} and R_{tester}.

4 Conclusions

EIS and SEM analysis were performed during exposure to 3.5%w NaCl aqueous solution on ZnO thin films deposited via magnetron sputtering under two different conditions of sub-

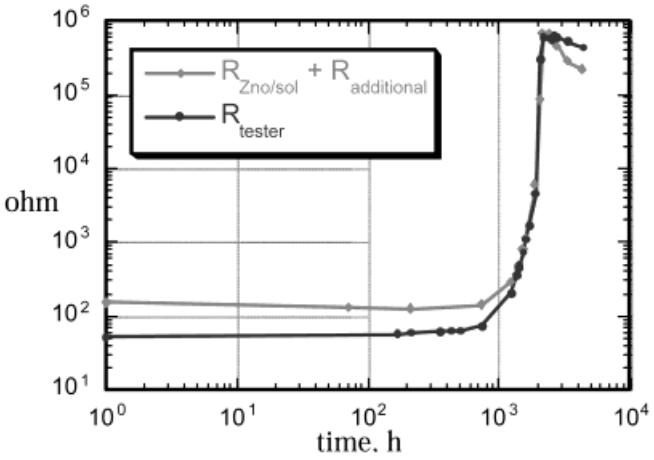

Fig. 11. Resistance of ZnO thin film measured by DC and EIS reported as a function of the exposure time to 3.5% NaCl aqueous solution

Abb. 11. Widerstand der ZnO-Schicht aus Gleichspannungs- und EIS-Messung als Funktion der Behandlungszeit in 3,5% iger wässriger NaCl-Lösung

strate temperature and chamber atmosphere (a-ZnO and b-ZnO).

Different surface morphology was observed by SEM analysis for a-ZnO and b-ZnO in the "as deposited" film condition. A double layered structure was observed for the a-ZnO. Both films showed nanocrystalline surface texture.

In the case of a-ZnO, SEM analysis showed a fast pitting driven degradation at early stages of exposure and a generalized film dissolution at later stages. In the case of b-ZnO, however, the degradation was driven by delamination and fracture of the film both at early and later stages of exposure. Significant dissolution of b-ZnO was not detected also at latest stages of exposure.

In spite of the different degradation mechanism, the impedance spectra of both a-ZnO and b-ZnO were described by common equivalent models and circuits. At the early stages of exposure a simple circuit, accounting for double layer capacitance, diffusion related phenomena and ZnO resistance, was employed. At latest stages, additional dipoles were employed in order to account for the voids in the semiconducting film (fractures or deep pits). Optimum agreement between experimental data and model prediction was found for both a-ZnO and b-ZnO at each stage of exposure.

The double layer capacitance was recognized as a measure of advancing degradation of the film. The appearing of a second time constant was recognized as flag to point the existence of fractures or deep pits in the film. The equivalent AC resistance measured by EIS showed good agreement with the DC resistance measured by simple tester. This resistance was assumed as a measure of the extensions of voids through the film.

5 Acknowledgments

The authors wish to gratefully acknowledge the EU – DGXII for the financial aid given within CEE grant JOR-.CT97-0140. One author, *D. B. Mitton*, wishes to express his gratitude to the University of Naples Federico II and to the Department of Materials and Production Engineering for supporting his collaboration on this project.

6 References

[1] *M. Izaki, T. Omi:* J. Electrochem. Soc. *144* (1997) 1949.
[2] *A. M. Chaparro, K. Ellmer, H. Tributsch:* El. Acta *44* (1999) 1655.
[3] *W. Hirschwald, P. Bonasieckwitz, L. Ernst, M. Grade, D. Hoffmann, S. Krebs, R. Littbarski, G. Neumann, M. Grunze, D. Kolb, H. J. Schultz:* Curr. Top. Mater. Sci. *7* (1981) 143.
[4] *C. M. Braun, A. Fujishima, K. Honda:* J. Electrochem. Soc. *1* (1986) 128.
[5] *Y. J. Kim, H. J. Kim:* Mat. Letters *41* (1999) 159.
[6] *J. F. Dewald:* J. Phys. Chem. Solids *14* (1960) 155.
[7] *J. F. Dewald:* Bell Syst. Tech. J. *39* (1960) 615.
[8] *Y. V. Pleskov:* In: Electric double layer on semiconductor electrodes, p. 291.
[9] *C. G. B. Brattain, W. H. Garrett:* Bell Syst. Tech. J. *34* (1955) 129.
[10] *J. Springer, E. M.Ozsan, A. Kazandjian, N. Niegisch, M. Mennig, H. Schmidt, J. Feichtinger, M. Hartmann, L. De Rosa, F. Bellucci:* In: Thin film solar module encapsulation processes for large area manufacturing, EEC IV RTD Framework Publishable Report, (1999).
[11] *N. Fujimura, T. Nishihara, S. Goto, T. Ito:* J. Cryst. Growth *115* (1991) 816.
[12] *G. Neumann, M. Grunze, D. Kolb, H. J. Schultz:* Curr. Top. Mater. Sci. *7* (1981) 143.
[13] *L. Sagalowicz, G. Fox:* J. Mat. Res. *14* (1999) 1876.
[14] *P. Spathis, I. Poulios:* Corr. Sci. *37* (1995) 673.
[15] *P. M. Verghese, D. Clarke:* J. Mat. Res. *14* (1999) 1039.
[16] *T. P. Dirkse:* J. Elctrochem. Soc. *133* (1986) 1656.

(Received: January 28, 2001) W 3553
Final version: May 29, 2001)